Mapping Seismocardiogram Characteristics to Hemorrhage Status and Vascular Pressure: A Novel Approach for Triage Assessment

Zeynep Deniz Gundogan[1] and Beren Semiz[2] [a]

[1]*Department of Electrical Engineering, Istanbul Technical University, Istanbul, Turkey*

[2]*Department of Electrical and Electronics Engineering, Koc University, Istanbul, Turkey*

Keywords: Seismocardiogram, Hemorrhage, Vascular Pressure, Biomedical Signal Processing.

Abstract: When a mass incident occurs, determining the severity of injuries and arranging the hospital triage are of great importance to increase the survival rates. This study aims to develop a seismocardiogram (SCG)-based triage assessment system by (i) distinguishing between different levels of exsanguination, and (ii) estimating the vascular pressure values recorded from various body locations for prioritizing the triage processes and monitoring vital parameters. In this project, publicly available *Wearable and Catheter-based Cardiovascular Signals During Progressive Exsanguination in a Porcine Model of Hemorrhage* dataset, which includes cardiovascular signals acquired through a catheter-based system and wearable sensors during progressive exsanguination, was used. First, temporal and spectral features were extracted from the SCG signals taken at different blood-loss levels from six Yorkshire swines. Hemorrhage severity assessment was then performed through multi-class classification leveraging *one vs. all* approach. As the second step, four different regression models were trained for each of the right atria, aortic root, femoral artery and pulmonary capillary locations to estimate the corresponding vascular pressure values. For hemorrhage severity assessment, the accuracy, sensitivity, precision and f1-score values were all calculated to be 0.96 for the best performing model (XGBoost). For the vascular pressure estimation, (mean-absolute-error and R^2) pairs were calculated to be (1.54, 0.94), (2.76, 0.58), (1.29, 0.87) and (0.95, 0.90) for aortic root, femoral artery, right atrium and pulmonary capillary models, respectively. Overall, this study introduced new use areas for the SCG signal, which can potentially be utilized in the development of continuous and non-invasive monitoring systems to prioritize the triage processes and track vital parameters.

1 INTRODUCTION

When a mass incident, such as an earthquake or public transport accident, occurs, determining the severity of injuries and arranging the hospital triage (i.e. order of treatment) are of great importance to increase the survival rates. Considering that the number of first responders and provided resources are limited, providing immediate and timely treatment to all victims is often not possible. Additionally, it is extremely important to monitor and detect deterioration risks in health status for preventing any follow-up complications. Therefore, there is a need for innovative approaches that can offer continuous hemodynamic monitoring to enable appropriate triage assessment.

As physiological signals emerge directly from the body, they hold valuable clinical information about the underlying physiological conditions and irreg-

ularities. In wearable device design, three of the most commonly used physiological signals can be listed as the electrocardiogram (ECG), photoplethysmogram (PPG), and seismocardiogram (SCG) waveforms. The SCG represents the mechanical activity of the heart resulting from the cardiac ejection and contraction, whereas the ECG acquires the electrical signal of the heart to assess rhythm and rate (Inan et al., 2014). Recent studies have shown that SCG signal can potentially be used in heart failure classification (Inan et al., 2018), myocardial contraction assessment (Tavakolian et al., 2012), respiration phase analysis (Imirzalioglu and Semiz, 2022; Pandia et al., 2012), valvular heart disease assessment (Erin and Semiz, 2023), metabolic equivalent of task score estimation (Tokmak and Semiz, 2022), systolic time interval and hemodynamic parameter estimation (Shandhi et al., 2019; Semiz et al., 2020). On the other hand, fluctuations in arterial blood volume during the cardiac

[a] https://orcid.org/0000-0002-7544-5974

cycle cause variations in the light absorption within the arteries, leading to the generation of PPG. Indeed, previous studies have shown that blood pressure, oxygen saturation and vascular resistance assessment can highly benefit from PPG analysis (cheol Jeong et al., 2018).

Among these signals, the researchers have recently found that the SCG signal is the most important modality in predicting decomposition (Kimball et al., 2021). Although there have been several studies on electronic triage tag development leveraging breathing rate, oxygen saturation, blood pressure, temperature, and heart rate assessment (Sakanushi et al., 2013; Rodriguez et al., 2014; Park, 2021; Grünerbel et al., 2023), there is no study focusing on the assessment of different levels of blood loss and corresponding vascular pressure values using solely the SCG signals. Hence, in this work, the fundamental aims were to investigate the relationship between blood loss levels and SCG signals, and to map the SCG signal characteristics to the vascular pressure values recorded from various body locations for prioritizing the triage processes and monitoring vital parameters.

The contributions of this study are threefold: For the first time, (i) SCG signal characteristics have been leveraged to distinguish between different levels of exsanguination, which can potentially accelerate the triage processes, (ii) SCG signal characteristics have been used to estimate the femoral artery, aortic root, right atrium and pulmonary capillary wedge pressure values to achieve continuous vascular pressure monitoring, (iii) it has been shown that the temporal characteristics of the SCG signal has relatively higher importance compared to the spectral ones in the case of hemorrhage assessment. Overall, the study introduces new use areas for the SCG signal, which can potentially be utilized in the development of continuous and non-invasive monitoring systems to prioritize the triage processes and track vital parameters.

2 MATERIALS AND METHODS

2.1 Dataset Description

2.1.1 Experimental Protocol

In this project, publicly available *Wearable and Catheter-based Cardiovascular Signals During Progressive Exsanguination in a Porcine Model of Hemorrhage* dataset was used (Zia et al., 2020a). The dataset contains cardiovascular signals acquired through a catheter-based system and wearable sensors during progressive exsanguination in a porcine model

of hemorrhage. The signals from the wearable sensors (seismocardiogram, electrocardiogram and photoplethysmogram) were acquired through BIOPAC MP160 system (BIOPAC Systems, Inc., Goleta, CA, USA). On the other hand, vascular pressure values from the aortic arch, femoral artery, right atrium and pulmonary capillary locations were collected with the catheter-based setup. Data from the catheters were acquired through the ADInstruments Powerlab 8/35 system. All signals were sampled at 2 kHz.

The study was conducted on 6 Yorkshire swines (3 castrated female, 3 male, weight: 51.5-71.4 kg, age: 114-150 days). Each swine underwent a health assessment examination and no other exclusion criteria was designated in the study. Anesthesia was administered with xylazine and telazol, and sustained via inhaled isoflurane during mechanical ventilation. During the experimental protocol, blood was drained through an arterial line at four levels (7%, 14%, 21%, and 28%) to induce hypovolemia. After every stage of blood loss, the process of exsanguination was temporarily halted for nearly 5-10 minutes so that the cardiovascular functions could return to normal. It should be noted that the experimental protocol was terminated at different blood levels for each pig as cardiovascular collapse was reached at different levels. More specifically, pig 5 reached 14% blood volume loss; pigs 1, 3, and 4 reached 21% blood volume loss; and pigs 2 and 6 reached 28% blood volume loss. These levels were visualized in Fig. 1(b).

2.1.2 Pre-Processing and Data Preparation

First, the signals were filtered with finite impulse response (FIR) band-pass filters with the following cut-off frequencies: SCG (1-40 Hz), ECG (0.5-40 Hz), PPG and catheter-based pressure signals (0.5-10 Hz). The signals were then segmented into individual beats using the R-peak locations of the ECG signal. Resulting segments were truncated into a length of 1000 samples (500 ms), except the third pig (1500 samples, 750 ms) due to relatively longer left ventricular ejection time. The catheter-based pressure signals were also truncated in a similar way.

Analysis pipeline is presented in Fig. 1(a). Two different analyses, hemorrhage severity assessment and vascular pressure estimation, were performed using the SCG signals taken from the dorso-ventral axis. For hemorrhage severity assessment, blood-loss levels at the time of each SCG beat were available as a separate vector. For the vascular pressure estimation analysis, the average of 1000 pressure samples was taken to have one single value for each pressure location. By this way, each SCG beat could be represented by one pressure value for each of the aortic
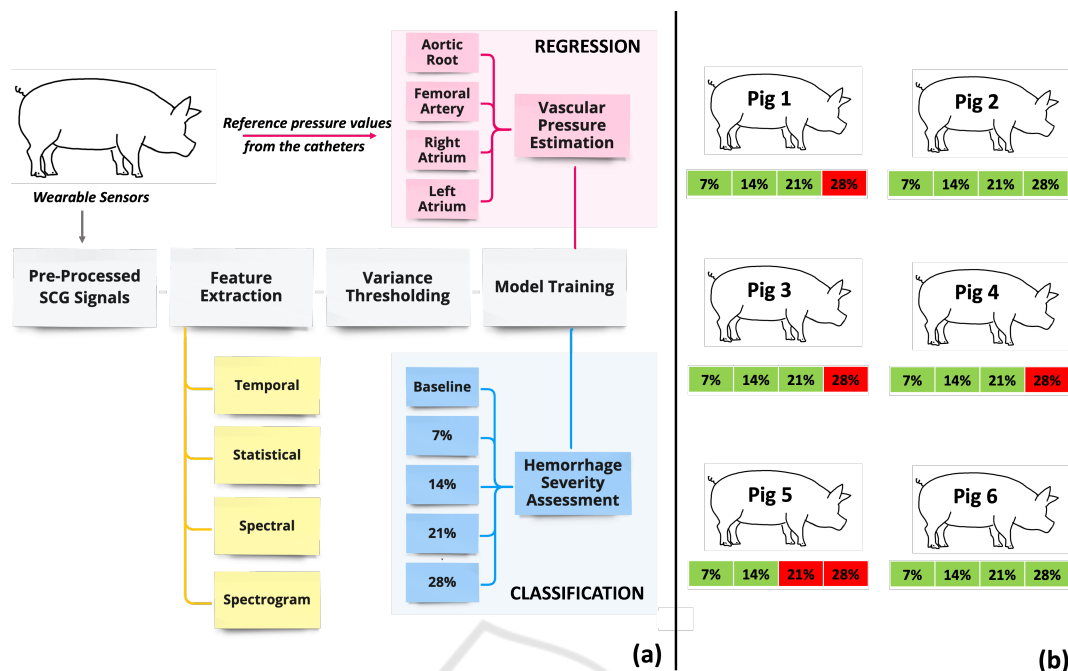
Figure 1: (a) Analysis pipeline (b) *Green color*: Blood loss levels that the pigs could reach, *Red color*: Blood loss levels that the pigs could not reach due to cardiovascular collapse.

arch, femoral artery, right atrium and pulmonary capillary locations.

2.2 Feature Extraction

Based on the previous studies, SCG analysis can highly benefit from time domain analysis, as valleys and peaks correspond to specific cardiovascular events in cardiac cycle (such as mitral closing (MC), aortic opening (AO), etc.) (Semiz et al., 2020). On the other hand, recent studies have revealed that spectral content of the SCG signals also contains salient information regarding underlying physiological events and pathologies (Erin and Semiz, 2023). Hence, each SCG signal segment was analyzed both in temporal and spectral domains. The sets of features are detailed in the following subsections.

2.2.1 Temporal Domain Analysis

For temporal domain analysis, energy, zero crossing rate, entropy and peak-location features were computed for each SCG segment. While energy corresponds to the total energy (i.e. sum of squared magnitudes of the samples), energy entropy assesses the abrupt changes observed in the signal energy. On the other hand, zero crossing rate measures the sign-change rate and used to evaluate the overall noise level. In addition to these three temporal features, the first three minima and maxima locations and ampli-

tudes were computed. This step resulted in an additional 12 features (6 amplitude and 6 location values). In the analysis, the valleys and peaks were not associated with particular cardiac events such as AO, MC, etc. This is due to two reasons - first, the SCG signals exhibit significant variability among different subjects, making it challenging to detect those points precisely. Second, the shape of the SCG signal changes depending on the sensor's location or the subject's posture (Hersek et al., 2019).

Additionally, statistical features were calculated for each segment. As statistical features, mean, root mean square, variance, satandard deviation, skewness and kurtosis were extracted. After computing the aforementioned features, a matrix $\mathbf{T}_i$ was generated for time domain features where each row corresponds to one segment, i, and each column represents one feature for each segment i. Overall, there were 21 temporal features extracted from each segment.

2.2.2 Spectral Domain Analysis

Following temporal analysis, spectral analysis was performed on the SCG segments. To that aim, spectral entropy, rolloff, spread and centroid values were computed for each segment i. While spectral entropy represents the complexity of the spectrum rolloff corresponds to the frequency below which a certain percentage of the signal energy is accumulated. Conversely, spectral centroid and spread pertain to the

center of mass and frequency distribution of the spectrum, respectively.

In addition to the aforementioned four spectral features, spectrogram analysis was employed. Spectrogram is used to investigate how the frequency characteristics of a non-stationary signal change with time. As the original function outputs frequency, time and coefficient values together, the average coefficients for each frequency band were computed over time and then stored as a vector. In total 129 spectrogram coefficients were extracted from each segment. After computing the aforementioned features, a matrix $\mathbf{S}_i$ was generated for spectral domain features where each row corresponds to one segment, i, and each column represents one feature for each segment i. Overall, there were 133 spectral features extracted from each segment.

2.2.3 Dataframe Generation

In total, there were 154 features (21 temporal and 133 spectral) extracted from each SCG segment. For convenience of feature selection and model training, one single data frame was created using these features. In the dataframe, each row was corresponding to one SCG segment i, whereas the columns were including the extracted features (time domain $\mathbf{T}_i$ and spectral domain $\mathbf{S}_i$ matrices). In addition to the feature columns, five additional columns were added to include blood-loss level labels (b_i) and the reference aortic root ($p1_i$), femoral artery ($p2_i$), right atria ($p3_i$) and pulmonary capillary wedge ($p4_i$) pressure values. Blood-loss levels were determined as 0, 1, 2, 3, 4 representing 0% (baseline), 7%, 14%, 21%, and 28% blood-loss levels, respectively. Overall, the dataframe was structured as follows: $[\mathbf{T}_i, \mathbf{S}_i, b_i, p1_i, p2_i, p3_i, p4_i]$.

2.2.4 Variance Thresholding

To prevent curse of dimensionality caused by high number of features, feature selection was applied on the 154 features extracted. As the feature selection method, variance thresholding, which seeks to eliminate features with variance values that fall below a specific threshold, was chosen. Since any feature's variance and level of predictive ability are correlated, features with smaller variance convey relatively less information (Bommert et al., 2020). In accordance with the previous study, threshold value was determined as 0.0001 (Erin and Semiz, 2023). Features below this threshold were masked as *False* and dropped, whereas the remaining features (which were above the threshold) were masked as *True* and kept in the analysis.

2.3 Model Training

Under model training, two different tasks were implemented: hemorrhage severity assessment and vascular pressure estimation. As detailed in Sec. 2.2.3, for hemorrhage severity classification, blood-loss levels were determined as 0, 1, 2, 3, 4 representing 0% (baseline), 7%, 14%, 21%, and 28% blood-loss levels, respectively. On the other hand, for vascular pressure estimation, four different regression models were trained for each of the aortic root, right atrium, femoral artery and pulmonary capillary wedge pressure estimation tasks. Both for hemorrhage severity assessment and vascular pressure assessment, four different models were trained and corresponding performance values were compared. It should be noted that machine learning models were leveraged instead of deep learning approaches due to the limited sample size.

- **Multi Layer Perceptron (MLP):** MLP falls under artificial neural networks composed of multiple layers of neurons (i.e., nodes), which are interconnected via weighted connections. From input layer to output layer, hidden layers perform complex transformations on the data. More specifically, each neuron in hidden layers computes weighted sum of the inputs, employs non-linear activation function and transfers the result to the following layer. The weights of these neuron connections are learned and updated during training through back-propagation (Bishop et al., 1995).

- **Support Vector Machines (SVM):** SVM aims to find the best separating hyperplane while maximizing the margin between the classes. In this context, the margin corresponds to the distance between the hyperplane and closest data points from different classes. SVM can also be used in regression tasks where the aim is to find the best hyperplane that minimizes the sum of the distances between the predicted and actual values (Noble, 2006).

- **Random Forest (RF):** RF is a type of ensemble methods where instead of using a single tree, it involves generating multiple trees by randomly selecting subsets from the original dataset. These trees are trained separately and in parallel, and their individual predictions are combined by averaging them to produce the final predicted target value (Breiman, 2001).

- **Extreme Gradient Boosting (XGBoost):** XGBoost also belongs to the ensemble methods category, more specifically the gradient boosting algorithm. This approach involves using multiple

estimators simultaneously instead of a single estimator to predict a variable. The algorithm trains numerous decision trees in a sequential manner, enabling the model to forecast the leftover errors from the previous round and enhance its performance progressively (Chen and Guestrin, 2016; Friedman, 2001).

2.3.1 Hemorrhage Severity Assessment

In the classification task, the idea was to assess the performance of the features extracted from the SCG signal in distinguishing between different blood loss levels. Using the features remained following variance thresholding, four different classification models were trained using MLP, SVM, RF and XGBoost. As explained in Section 2.1.1 and Fig. 1(b), the experimental protocol was terminated at different blood levels as each pig reached cardiovascular collapse at different levels. While pigs 1, 3, and 4 reached 21% blood volume loss, pigs 2 and 6 could reach 28% blood volume loss, and pig 5 could only reach 14% blood volume loss. Thus, there was an imbalance within the dataset: pigs 2 and 6 indeed had data corresponding to each phase, whereas the other pigs were missing one or two labels. Hence, instead of building a leave-one-subject-out cross-validation framework, k-fold cross validation was employed during model training to prevent the bias that will occur across folds.

The data was first split into k number of subgroups (folds). In each iteration, one fold was left out for testing and the model was trained with the remaining (k-1) folds. The iterations continued until every split was used for testing. In this project, k was set to 5. On the other hand, the depth value used in XGBoost and RF classifiers were chosen as 10 through grid search. Indeed this value was in accordance with the one used in (Zia et al., 2020b). For severity classification, *one vs. all* approach was leveraged and the models' performance was assessed using accuracy, recall, precision and f1-scores. The corresponding equations were listed in Equations 1, 2, 3, 4, respectively (*TN: true negatives, TP: true positives, FN: false negatives, FP: false positives*).

$$Accuracy = \frac{TP + TN}{TP + TN + FP + FN} \tag{1}$$

$$Recall = \frac{TP}{TP + FN} \tag{2}$$

$$Precision = \frac{TP}{TP + FP} \tag{3}$$

$$f_1 score = 2 * \frac{precision * recall}{precision + recall} \tag{4}$$

2.3.2 Vascular Pressure Estimation

In the regression part, the relationship between the catheter-based pressure values and SCG-based features was examined. Similar to the classification task, MLP, SVM, RF and XGBoost were used to estimate the vascular pressures from different locations. Model validation was again employed through 5-fold cross validation and the depth value used in XGBoost and RF regressors were determined using grid search. The best option for right atrium pressure, aortic root pressure, and pulmonary capillary wedge pressure was found to be 10, whereas the best depth option for femoral artery pressure was determined as 8. The performance of the regressors was evaluated through mean absolute error (MAE) and coefficient of determination (R^2) metrics. The corresponding equations were listed in Equations 5 and 6, respectively (y_{true}: *actual values*, y_{pred}: *predicted values*, y_{mean}: *mean of the actual values*).

$$MAE = \frac{\sum_{i=1}^{n} |y_{pred,i} - y_{true,i}|}{n} \tag{5}$$

$$R^2 = 1 - \frac{\sum_{i=1}^{n} (y_{true,i} - y_{pred,i})^2}{\sum_{i=1}^{n} (y_{true,i} - y_{mean})^2} \tag{6}$$

2.4 Feature Importance Ranking

To gain a better understanding of which features are most important for classification, it is necessary to calculate the relative weight of each feature in the model. This can directly be achieved through the use of decision trees trained by the XGBoost classifier as the features to split are determined based on the greatest reduction in loss. Each decision tree ranks the features based on their importance in the resulting classification algorithm. After running all the trees in the model, the relative importance of the features can thus be determined by averaging the importance scores obtained from each tree. These scores are then used to obtain the final relative feature importance ranking.

As the best performing model was XGBoost, it was used to evaluate which features among the remaining ones were most relevant for distinguishing between different blood loss levels. To that aim, a second XGBoost classifier was trained, this time using data from all pigs. The resulting model was then used to calculate the feature importance scores. Since the objective was not to assess the model's ability to generalize, no separate testing set was required.

Table 1: Remaining features after variance thresholding *(max: maximum, min: minimum, amp: amplitude, loc: location, rms: root mean square).*

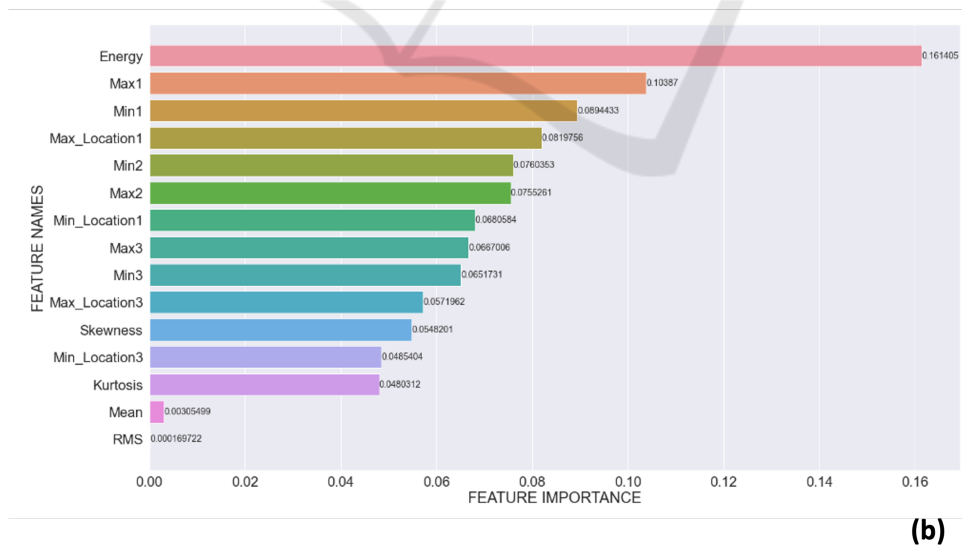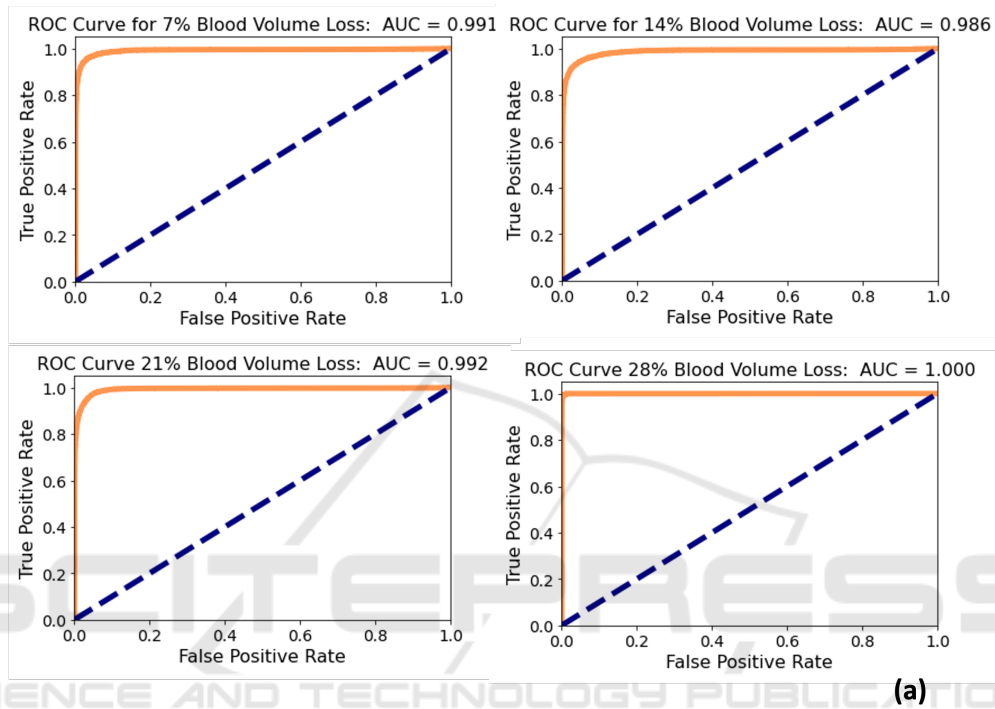| Remaining 17 Features					
First Max Amp	First Max Loc	First Min Amp	First Min Loc	Energy	Skewness
Second Max Amp	Second Max Loc	Second Min Amp	Second Min Loc	RMS	Kurtosis
Third Max Amp	Third Max Loc	Third Min Amp	Third Min Loc	Mean	

(a)

(b)

Figure 2: (a) Receiver Operating Characteristic (ROC) Curves for different blood volume loss stages. (b) Normalized feature importance values for the first 15 features out of 17 *(max: maximum, min: minimum, amp: amplitude, rms: root mean square).*

Table 2: Performance metrics for different machine learning models.

Classification (Accuracy)				
	Random Forest	**XGBoost**	**MLP**	**SVM**
Blood-Level Classification	0.92	**0.96**	0.55	0.45
Regression (R^2)				
	Random Forest	**XGBoost**	**MLP**	**SVM**
Right Atrium Pressure	0.86	**0.87**	0.56	0.24
Aortic Root Pressure	0.90	**0.94**	0.56	0.25
Femoral Artery Pressure	**0.60**	0.58	0.32	0.14
Pulmonary Capillary Wedge Pressure	0.85	**0.90**	0.34	0.21

Table 3: XGBoost classification and regression results.

XGBoost Classification				
	Accuracy	**Precision**	**Recall**	**F1-Score**
Blood-Level Classification	0.96	0.96	0.96	0.96
XGBoost Regression				
	R^2		**Mean Absolute Error**	
Right Atrium Pressure	0.87		1.29	
Aortic Root Pressure	0.94		1.54	
Femoral Artery Pressure	0.58		2.76	
Pulmonary Capillary Wedge Pressure	0.90		0.95	

3 RESULTS

3.1 Feature Selection with Variance Thresholding

In this project, both temporal and spectral domain analyses were leveraged as previous studies have shown the success of each in various applications. In total there were 154 features and this number decreased to 17 following variance thresholding. The remaining features are presented in Table 1. As seen, only the temporal ones, i.e. time domain and statistical features, appeared in the remaining 17 features and none of the spectral features were included in the resulting set.

3.2 Hemorrhage Severity Assessment

As detailed in Section 2.3.1, four classification models were trained using the remaining 17 features for hemorrhage severity assessment. The models' performance was first evaluated with the accuracy metric. As reported in Table 2, RF, XGBoost, MLP and SVM models resulted in an accuracy of 0.92, 0.96, 0.55 and 0.45, respectively. Out of the four models, XGBoost was found to be the best performing one. For the XG-Boost classifier, each of the accuracy, recall, precision and f1-score was also calculated to be 0.96, as reported in Table 3.

To investigate how the model behaves for different threshold values, receiver operating characteristic (ROC) curve for each blood level was plotted. For 7%, 14%, 21% and 28% blood loss levels, the area under curve (AUC) values were calculated to be 0.991, 0.986, 0.992 and 1.000, respectively (Fig. 2(a)).

3.3 Vascular Pressure Estimation

Under the vascular pressure estimation task, regression models were trained for each of the aortic root, femoral artery, right atrium and pulmonary capillary wedge pressure values. For each location, four different models, RF, XGBoost, MLP and SVM were leveraged similar to the classification task. For the right atrium, aortic root and pulmonary capillary locations, XGBoost resulted in the best accuracy values (0.87, 0.94 and 0.90, respectively). On the other hand, for the femoral artery pressure estimation, RF slightly outperformed XGBoost (0.60 vs. 0.58). Still, XGBoost was selected as the final model for all four locations. As presented in Table 3, MAE values were calculated to be 1.29, 1.54, 2.76 and 0.95 for right atrium, aortic root, femoral artery and pulmonary capillary models, respectively. The scatter plots representing the predicted and actual vascular pressure values with the corresponding R^2 results are presented in Fig. 3.
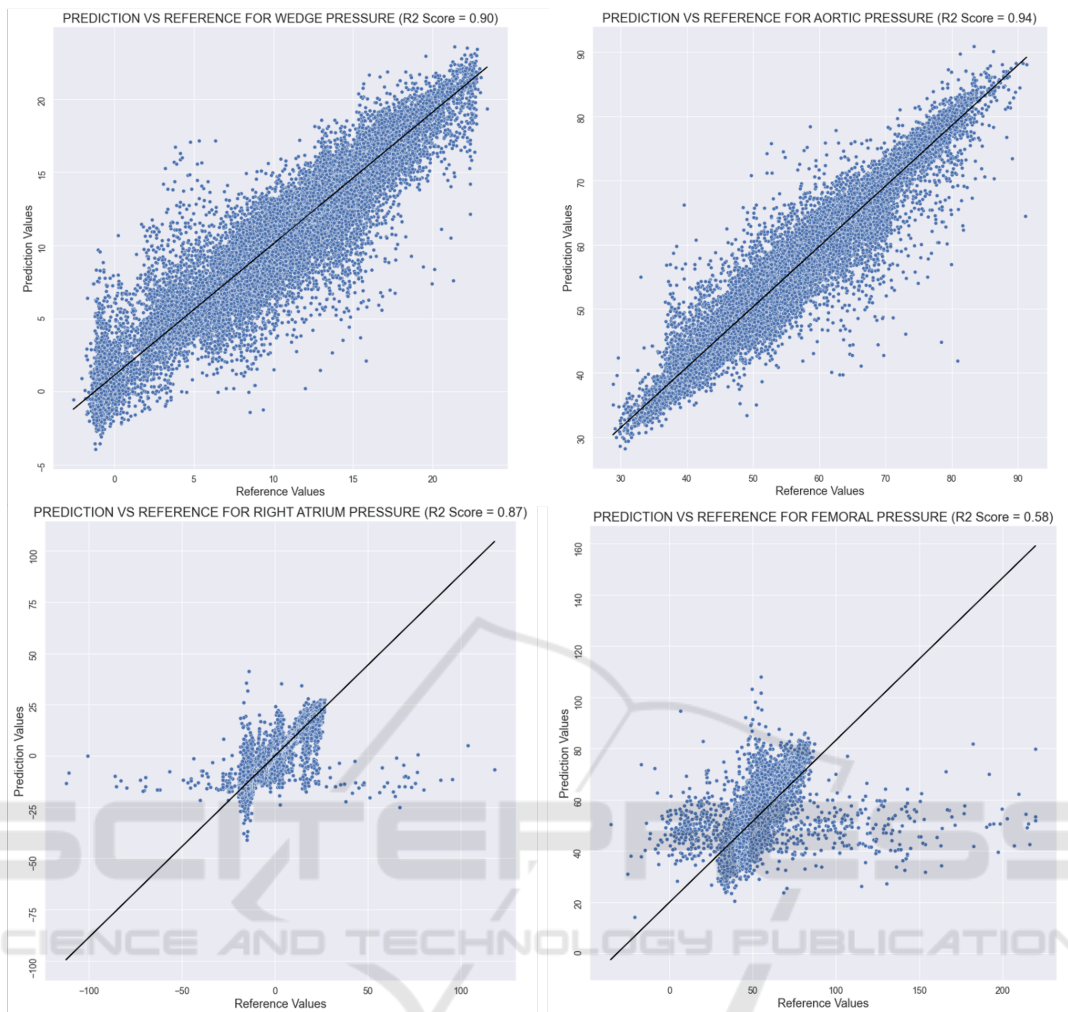
Figure 3: Regression plots for each pressure location. Black lines correspond to the best fit lines.

3.4 Feature Importance Ranking

As explained in Section 2.4, feature importance ranking was applied using the XGBoost model on the remaining 17 temporal features. The normalized importance scores of the first fifteen out of seventeen features are shown in Fig. 2(b). As seen, energy, first maximum amplitude (Max 1) and first minimum amplitude (Min 1) appeared as the top three most important features. On the other hand, the statistical features appeared in the lower end on the importance ranking.

4 DISCUSSION

4.1 Model Training and Interpretation

Both for the hemorrhage severity assessment and vascular pressure estimation tasks, 5-fold cross-validation was leveraged instead of leave-one-subject-out cross-validation (LOSO-CV). Since the pigs reached cardiovascular collapse at different blood-loss levels, some pigs did not have any data relating to 21% or 28% blood loss, as previously shown in Fig. 1(a). Due to this imbalance, the models would not be able to learn properly if LOSO-CV was used; hence, 5-fold cross-validation was employed in all tasks.

Overall, for both classification and regression tasks, high performance metrics were obtained. Among different vascular pressure values, the worst performing model was the one estimating the femoral

artery pressure. Considering that the accelerometer acquiring the SCG signal was placed on the mid-sternum of the pig, femoral artery was at a relatively distal location compared to remaining three pressure locations. Indeed, when the pressure measurements are taken further from the aorta, a relatively higher systolic pressure, lower end diastolic pressure and later arrival of pulse have been observed (Chambers et al., 2019). Hence, collecting the SCG signals from the mid-sternum and trying to estimate femoral artery pressure would naturally be prone to more intra-subject variability compared to other three locations.

4.2 Feature Interpretation

As previously explained, the temporal features outperformed spectral features in terms of relative importance in hemorrhage assessment. Having amplitude-related features as the most important ones was indeed consistent with the underlying physiological events. It has previously been shown that there is salient information regarding stroke volume in SCG amplitude characteristics as the SCG signal represents the local vibrations originating from ejection of blood in each contraction (Semiz et al., 2020). Similarly, in another study, it has been shown that the percent change in post-hemorrhage cardiac output and percent reduction in blood volume had a linear relationship (Chien and Billig, 1961). Based on these studies, having amplitude features as the most important ones in distinguishing between different blood-loss levels was indeed consistent with the literature.

4.3 Limitations and Future Work

There were several limitations in the proposed work. First, the dataset size was relatively small (including 6 pigs). In addition, there was an imbalance in the number of samples available for each blood-loss level as the experimental protocol was terminated at different blood levels for each pig. Hence, future work will focus on testing the proposed features and pipelines in larger datasets for assessing the generalizability of the models.

5 CONCLUSION

The main objectives of this study were to explore how blood loss levels relate to the SCG signals, and to establish a correlation between the characteristics of SCG signals and the vascular pressure values obtained from various parts of the body. It was hypoth-

esized that such a system could be useful in prioritizing triage processes and monitoring critical parameters. For hemorrhage severity classification, SCG data taken during different blood loss levels were classified using *one vs. all* approach. Each of the precision, recall and f1-score was calculated to be 0.96, and temporal features outperformed spectral ones in terms of added information. On the other hand, for vascular pressure assessment, MAE values were calculated to be 1.29, 1.54, 2.76 and 0.95 for right atrium, aortic root, femoral artery and pulmonary capillary models, respectively. Out of these pressure locations, femoral artery pressure estimation resulted in the worst performance with an R^2 value of 0.58 due to its distal location relative to mid-sternum. Overall, this study introduced new use areas for the SCG signal, which can be utilized in the development of continuous and non-invasive monitoring systems to prioritize the triage processes and track vital parameters.

REFERENCES

Bishop, C. M. et al. (1995). *Neural networks for pattern recognition*. Oxford university press.

Bommert, A., Sun, X., Bischl, B., Rahnenführer, J., and Lang, M. (2020). Benchmark for filter methods for feature selection in high-dimensional classification data. *Computational Statistics & Data Analysis*, 143:106839.

Breiman, L. (2001). Random forests. *Machine learning*, 45:5–32.

Chambers, D., Huang, C., and Matthews, G. (2019). *Arterial Pressure Waveforms*, page 155–157. Cambridge University Press, 2 edition.

Chen, T. and Guestrin, C. (2016). Xgboost: A scalable tree boosting system. In *Proceedings of the 22nd acm sigkdd international conference on knowledge discovery and data mining*, pages 785–794.

cheol Jeong, I., Bychkov, D., and Searson, P. C. (2018). Wearable devices for precision medicine and health state monitoring. *IEEE Transactions on Biomedical Engineering*, 66(5):1242–1258.

Chien, S. and Billig, S. (1961). Effect of hemorrhage on cardiac output of sympathectomized dogs. *American Journal of Physiology-Legacy Content*, 201(3):475–479.

Erin, E. and Semiz, B. (2023). Spectral analysis of cardiogenic vibrations to distinguish between valvular heart diseases.

Friedman, J. H. (2001). Greedy function approximation: a gradient boosting machine. *Annals of statistics*, pages 1189–1232.

Grünerbel, L., Heinrich, F., Zett, O., Axelsson, K., and Schumann, M. (2023). Towards an intelligent triage bracelet: A conceptual study of a semi-automated pre-

hospital triage algorithm and the integration of blood pressure measurement.

Hersek, S., Semiz, B., Shandhi, M. M. H., Orlandic, L., and Inan, O. T. (2019). A globalized model for mapping wearable seismocardiogram signals to whole-body ballistocardiogram signals based on deep learning. *IEEE journal of biomedical and health informatics*, 24(5):1296–1309.

Imirzalioglu, M. and Semiz, B. (2022). Quantifying respiration effects on cardiac vibrations using teager energy operator and gradient boosted trees. In *2022 44th Annual International Conference of the IEEE Engineering in Medicine & Biology Society (EMBC)*, pages 1935–1938. IEEE.

Inan, O. T., Baran Pouyan, M., Javaid, A. Q., Dowling, S., Etemadi, M., Dorier, A., Heller, J. A., Bicen, A. O., Roy, S., De Marco, T., et al. (2018). Novel wearable seismocardiography and machine learning algorithms can assess clinical status of heart failure patients. *Circulation: Heart Failure*, 11(1):e004313.

Inan, O. T., Migeotte, P.-F., Park, K.-S., Etemadi, M., Tavakolian, K., Casanella, R., Zanetti, J., Tank, J., Funtova, I., Prisk, G. K., et al. (2014). Ballistocardiography and seismocardiography: A review of recent advances. *IEEE journal of biomedical and health informatics*, 19(4):1414–1427.

Kimball, J. P., Zia, J. S., An, S., Rolfes, C., Hahn, J.-O., Sawka, M. N., and Inan, O. T. (2021). Unifying the estimation of blood volume decompensation status in a porcine model of relative and absolute hypovolemia via wearable sensing. *IEEE Journal of Biomedical and Health Informatics*, 25(9):3351–3360.

Noble, W. S. (2006). What is a support vector machine? *Nature biotechnology*, 24(12):1565–1567.

Pandia, K., Inan, O. T., Kovacs, G. T., and Giovangrandi, L. (2012). Extracting respiratory information from seismocardiogram signals acquired on the chest using a miniature accelerometer. *Physiological measurement*, 33(10):1643.

Park, J. Y. (2021). Real-time monitoring electronic triage tag system for improving survival rate in disaster-induced mass casualty incidents. In *Healthcare*, volume 9, page 877. MDPI.

Rodriguez, D., Heuer, S., Guerra, A., Stork, W., Weber, B., and Eichler, M. (2014). Towards automatic sensor-based triage for individual remote monitoring during mass casualty incidents. In *2014 IEEE international conference on bioinformatics and biomedicine (BIBM)*, pages 544–551. IEEE.

Sakanushi, K., Hieda, T., Shiraishi, T., Ode, Y., Takeuchi, Y., Imai, M., Higashino, T., and Tanaka, H. (2013). Electronic triage system for continuously monitoring casualties at disaster scenes. *Journal of Ambient Intelligence and Humanized Computing*, 4:547–558.

Semiz, B., Carek, A. M., Johnson, J. C., Ahmad, S., Heller, J. A., Vicente, F. G., Caron, S., Hogue, C. W., Etemadi, M., and Inan, O. T. (2020). Non-invasive wearable patch utilizing seismocardiography for perioperative use in surgical patients. *IEEE journal of biomedical and health informatics*, 25(5):1572–1582.

Shandhi, M. M. H., Semiz, B., Hersek, S., Goller, N., Ayazi, F., and Inan, O. T. (2019). Performance analysis of gyroscope and accelerometer sensors for seismocardiography-based wearable pre-ejection period estimation. *IEEE journal of biomedical and health informatics*, 23(6):2365–2374.

Tavakolian, K., Portacio, G., Tamddondoust, N. R., Jahns, G., Ngai, B., Dumont, G. A., and Blaber, A. P. (2012). Myocardial contractility: A seismocardiography approach. In *2012 Annual International Conference of the IEEE Engineering in Medicine and Biology Society*, pages 3801–3804. IEEE.

Tokmak, F. and Semiz, B. (2022). Unveiling the relationships between seismocardiogram signals, physical activity types and metabolic equivalent of task scores. *IEEE Transactions on Biomedical Engineering*.

Zia, J., Kimball, J., Hahn, J.-O., Rolfes, C., and Inan, O. (2020a). Wearable- and catheter-based cardiovascular signals during progressive exsanguination in a porcine model of hemorrhage.

Zia, J., Kimball, J., Rolfes, C., Hahn, J.-O., and Inan, O. T. (2020b). Enabling the assessment of trauma-induced hemorrhage via smart wearable systems. *Science advances*, 6(30):eabb1708.